Unfolding complex dynamics of sagged cables around a divergence-Hopf bifurcation: experimental results and phenomenological model

Rocco Alaggio[1] and Giuseppe Rega[2]

[1] *Dipartimento di Ingegneria delle Strutture, delle Acque e del Terreno, Università dell'Aquila*
E-mail: *rocco.alaggio@univaq.it*
[2] *Dipartimento di Ingegneria Strutturale e Geotecnica, Sapienza Università di Roma*
E-mail: *giuseppe.rega@uniroma1.it*

Keywords: Experimental bifurcation scenario, phenomenological model, sagged cable

SUMMARY

An experimental bifurcation scenario to low-dimensional homoclinic chaos in the finite amplitude forced dynamics of a sagged cable is characterized in-depth, referring the relevant regular and non-regular dynamics to a canonical scenario from dynamical systems theory. A feedback between experiments and theory allows us to build a consistent phenomenological model: the unfolding of a canonical bifurcation normal form is used to produce an highly degenerated periodically perturbed bifurcation set in an enlarged parameter space where the effects of material damping and forcing asymmetry are evidenced.

1 BACKGROUND AND MOTIVATION

Finite amplitude dynamics of suspended cables have been addressed in the last two decades by variably refined theoretical models through purely analytical, numerical or mixed treatments [1]. However, understanding the actual nonlinear behaviour of suspended cables through also physical models is important both for validating theoretical predictions and for detecting new or complex phenomena associated with system nonlinearities but often un-modelled in theoretical analyses.

Quite a systematic analysis of experimental nonlinear cable dynamics has been accomplished in a few papers dealing with a hanging cable/mass system subjected to different harmonic motions of the supports and realizing, for relatively low excitation frequencies, a fairly reliable model of bare suspended cable. Focusing on the transition to complex response under various external and internal resonance conditions, bifurcation mechanisms have been characterized by properly reconstructing the system dynamics from experimental measurements [2, 3]. Reconstructed attractors and underlying manifolds have been studied via different experimental techniques, i.e., delay embedding and proper orthogonal decomposition, focused at identifying mechanically meaningful classes of motion and the associated mechanisms of transition to chaos. Particular interest has been devoted to highlight the possible occurrence of low-dimensional complex responses, which is of major interest for identifying reduced (and minimal) theoretical models able to describe the complex dynamics of the experimental system.

An overview on the richness and robustness of two different – quasiperiodic and homoclinic – bifurcation scenarios to chaos occurring in various regions of control parameter space, along with the involved proper orthogonal modes (POMs), is summarized in Table I, making reference to features of support motion, external resonance condition, and cable dynamic properties [3].

For the slacker cable, quasiperiodic transition to chaos via breakdown of regular dynamics on 3D-tori is robust at primary resonance under in-phase support motion, whereas it competes with

the homoclinic bifurcation scenario at 1/2-subharmonic resonance under out-of-phase motion. In turn, this latter scenario is definitely robust near primary resonances of 1:1 internally resonant VnHn-type couples of modes (V=vertical, in-plane; H=horizontal, out-of-plane; n=2-5; n=odd, symmetric; n=even, antisymmetric) for both the slacker and the crossover cable. However, while the quasiperiodic transition to chaos through a tori breakdown has been addressed quite exhaustively and satisfactorily [2], only some preliminary, yet promising, results were obtained as regards the quite *general* scenario seemingly involving two main – though variable – POMs in the global bifurcation of a homoclinic invariant set of the flow.

Thus, by focusing on the homoclinic bifurcation of a multiple internally resonant cable under anti-phase support motion at primary resonance, two main items are to be accomplished. (i) Going in-depth into its experimental characterization, by analysing the relevant peculiar and/or persistent bifurcation features, and by possibly tracing them back to a canonical scenario from dynamical systems theory; (ii) developing a phenomenological theoretical model able to reproduce the intrinsic features of the dynamical system and its overall bifurcation scenario. The first item, which involves a systematic physical investigation and the understanding of phenomena responsible for the onset of experimental non-regular dynamics, has been accomplished in [4].

In turn, developing a phenomenological bifurcation model relying on the normal form of bifurcation mechanisms known from dynamical system theory and properly modified to account for the specific features of the experimental system and response, can allow us to gain insight into the limits of some assumptions made in "classical" theoretical modelling of suspended cables. As a matter of fact, in the context of a profitable feedback between experiments and theory, such a phenomenological model can allow us to recognize the mechanical meaning of terms playing a meaningful role in the bifurcation mechanisms, thus paving the way towards the independent formulation of a theoretical reduced order cable model having all the necessary pre-requisites for possibly reproducing the experimentally observed phenomena. This second item is specifically accomplished in this paper.

Some main experimental results from the systematic investigation are summarized in Sect. 2, along with the unfolding of the relevant regular and non-regular dynamics within a reference bifurcation scenario. Then, the low-dimensional phenomenological model is presented in Sect. 3 by considering the O(2) symmetric nilpotent double-zero normal form, from which a highly degenerated bifurcation set is produced and then perturbed to obtain an enriched D4 normal form accounting for support motion. Finally, partial unfolding of the Z2 normal form describing the solely vertical support motion and capable to exhibit a bifurcation scenario comparable to the experimental one is presented in Sect. 4, with a few conclusions being given in Sect. 5.

Table I: Summary of results concerned with bifurcation to chaos scenarios.

Summary of nonregular regime zones, corresponding transition scenarios, and involved configuration variables – transition to non-regular dynamics

Cable	Support motion							
	In-phase external resonance condition				In opposition of phase external resonance condition			
	Primary		Subh. 1/2		Primary		Subh. 1/2	
	Scenario	Modes	Scenario	Modes	Scenario	Modes	Scenario	Modes
Slacker	QP	V1 H1 H2	HOM (HET)	V5 H5 V3 H3	HOM	V2 H2	HOM (QP)	V4 H4[a]
Crossover	No chaos		HOM	V5 H5 V3 H3	HOM	V2 H2	HOM	V4 H4

[a] V4 H4 $H1^T$ H2.

2 SUMMARY OF EXPERIMENTAL RESULTS AROUND A DIVERGENCE-HOPF BIFURCATION

System mechanical and geometrical properties of the experimental system (Fig. 1) realize a condition of 2:2:1 multiple internal resonance amongst the frequencies of first anti-symmetric in-plane (V2) and out-of-plane (H2) modes, and first symmetric out-of-plane (H1) mode. Previous non-systematic results allowed to conjecture that, when the first anti-symmetric in-plane mode is excited at primary resonance, a scenario involving the global bifurcation of an homoclinic invariant set could be responsible for transition to chaos with two dominant POMs resembling the linear modes V2 and H2 (Fig. 2) [3]. Thereafter, behavior charts in the frequency-amplitude excitation plane have been obtained within a systematic, thermally conditioned and controllable, experimental investigation made at different temperature (T) values. Two of them are depicted in Fig. 3: see [4] for a detailed discussion of the various classes of motion and of the relevant dynamic indicators reported in the tables. Overall, rich and complex responses do occur within the wide range wherein the directly forced one-mode solution P1M1 (label A) is unstable (Fig. 3).

The organizing role of a divergence-Hopf (d-H) codimension two bifurcation is evidenced in both charts, along with the effect played by the temperature (material hysteretic properties do depend on temperature). Varying the temperature entails the variation of the d-H forcing critical value and of the dimension of some response classes. However, though some differences occur between bifurcation diagrams, it is possible to inscribe them in the framework of the stability diagrams of the d-H normal form. The possible involvement of other POMs, besides V2 and H2, produces motion classes with augmented dimension but does not entails qualitative changes with respect to canonical bifurcation diagrams, i.e. topologically equivalent motion classes bifurcate following the canonical path even if they are embedded in higher order manifolds.

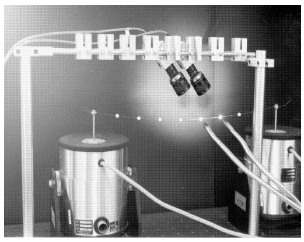

Figure 1: Experimental setup.

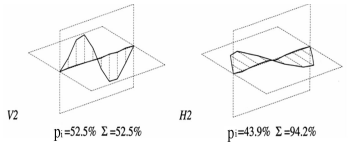

Figure 2: First two POMs inside the lower dimension chaotic region.

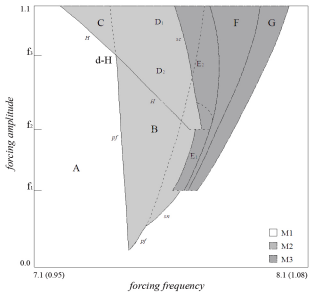

Zone		Attractor	Dimension			Modes
			De	D-T	poms	
A		P1M1	1	1	1	V_2
C		QP1M1	2	2	1	V_2
B		P1M2$^{(SC)}$	1	2^{R}	2	V_2 H_2
D1		QP2M2$^{(S)}$	2	2	2	V_2H_2
		QP2M2$^{(SC)}$	2	2	2	V_2H_2
D2		QP1M2$^{(SC)}$	2	2	2	V_2H_2
E1	(a)	QP1M3	2	3^{R}	3	$V_2H_2H_1$
	(b)	QP2M3	2	3^{R}	3	$V_2H_2H_1$
	←	P1M1	1	1	1	V_2
E2	(a)	QP1M3	2	3^{R}	3	$V_2H_2H_1$
	(c)	P2M3	1	3^{R}	3	$V_2H_2H_1$
← →	(d)	P1M1	1	1	1	V_2
F	(a)	CHM3	2.8		3	$V_2H_2H_1$
	(b)	P2M3	1	3^{R}	3	V_2H_2 H_1
	←	P1M1	1	1	1	V_2
G	(b)	P2M3	1	3^{R}	3	$V_2H_2H_1$
		P1M1	1	1	1	V_2

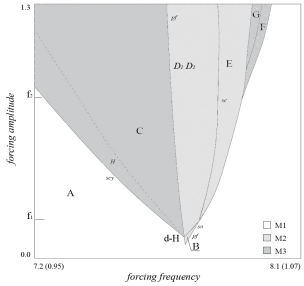

Zone	Attractor	Dimension			Modes
		De	D-T	poms	
A	P1M1	1	1	1	V_2
B	P1M1	1	2^{R}	2	V_2
C	QP1M1$^{(C2)(S)}$	2	2	1(+2)	$V_2(H_1V_1)$
D_1	QP1M2$^{(S)}$	2	2	2	V_2H_2
D_2	QP1M2$^{(SC)}$	2	2	2	V_2H_2
E	CHM2	2.3		2	V_2H_2
G	QP5M2	2	2	2	V_2H_2
F	CHM3	3.1		3	$V_2H_2H_1$
	P1M1	1	1	1	V_2

Figure 3: Qualitative behaviour chart and characterization of motion classes (left, T=12°C; right, T=4°C).

However, for even lower temperature, the overall scenario changes dramatically [4].

Results of a delay embedding reconstruction of phase space from a time series singled out from the chaotic motion CHM2 are reported in Fig. 4. Dynamics is organized by an unstable fixed point on the map characterized by a two-dimensional focus-stable manifold W^s and a one-dimensional saddle-unstable manifold W^u, and an invariant of the flow responsible for re-injection toward the fixed point. The fixed point on the second order Poincarè section corresponds to an unstable two-dimensional invariant of the flow resembling a formerly stable quasiperiodic motion ($QP1M2^{(SC)}$).

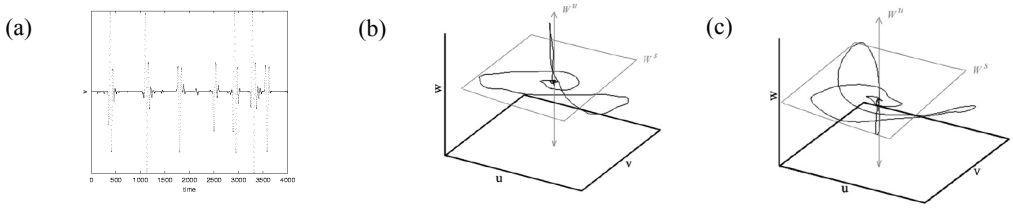

Figure 4: Time delay reconstruction: (a) time series, (b) and (c) projections of the second order Poincaré section of the reconstructed attractor show a typical homoclinic evolution.

2.1 *Schematic unfolding of regular and nonregular dynamics*

The experimental results allow to draw a robust unfolding of both *regular* and *nonregular* dynamics and to refer the overall bifurcation scenario to a canonical one in dynamical system theory. Indeed, the experimental scenario appears to be consistent with the unfolding of the dynamics in the neighbourhood of a d-H bifurcation point, provided the topological dimension of the observed periodically forced motion classes is reduced by one, i.e. if looking at the experimental Poincaré section. Due to the external and internal resonance features, the system dynamics in both regular and non-regular regime is essentially traceable to participation of two spatial shapes closely resembling the first two anti-symmetric linear modes.

It is worth observing that, besides the two main control parameters, excitation frequency and amplitude, varying the temperature as a further "external" control parameter allows us to highlight the strong role likely played by the material damping (which depends on temperature) in unfolding the experimental dynamics. Yet, a substantially invariant bifurcation scheme is seen to persist over the whole range of temperature variation, thus allowing us to refer to the theoretical unfolding provided by the low-dimensional bifurcation system represented by the d-H normal form.

In the *regular dynamics* regime, for growing frequency at temperatures $T \geq 6°C$, two most robust experimental bifurcation paths occur in the neighbourhood of d-H point, for forcing levels respectively higher and lower than the critical value:

$$\textit{(i)}\ P1M1 \xrightarrow[H]{} QP1M1 \xrightarrow[pf]{} QP1M2^{(S)} \xrightarrow[global]{} QP1M2^{(SC)} \xrightarrow[global]{} P1M1$$

$$\textit{(ii)}\ P1M1 \xrightarrow[pf]{} P1M2^{(SC)} \xrightarrow[H]{} QP1M2^{(SC)} \xrightarrow[global]{} P1M1$$

For the sake of comparing the unfolding of experimental results around d-H with theoretical scenarios, stability and bifurcation diagrams are sketched in Fig. 5. Solutions and bifurcations are described as follows, starting from the region *(a)* where only the anti-symmetric in-plane POM takes part in the response (focus fixed point P1M1).

Following an anti-clockwise path (corresponding to the former path (*ii*)) in Fig. 5a: (i) From *(a)* to *(e)*, P1M1 loses stability due to pitchfork to a couple of coexisting symmetric foci $P1M2^{(SC)}$ on a resonant two-torus. At pitchfork, the anti-symmetric out-of-plane experimental eigenfunction enters the response. Due to reflection symmetry, the system has solutions either self-symmetric

(prime $^{(S)}$) or being related in symmetric pairs (prime $^{(SC)}$). (ii) From *(e)* to *(d)*, the couple of symmetric foci P1M2$^{(SC)}$ bifurcates through Hopf to the couple of limit cycles QP1M2$^{(SC)}$.

Following a clockwise path (corresponding to the former path *(i)*) in Fig. 5b: (i) From *(a)* to *(b)*, stability of P1M1 is lost through Hopf and a limit cycle (QP1M1) settles down; in the schematic diagram of Fig. 5b, the unstable fixed point and a stable limit cycle are shown. (ii) From *(b)* to (*c*), a pitchfork bifurcation is trespassed and two new unstable fixed points add to phase space. The pitchfork drives the out-of-plane anti-symmetric experimental eigenfunction into the response. Phase space is characterized by three unstable fixed points and a cross-well limit cycle (QP1M2$^{(S)}$). (iii) From *(c)* to *(d)*, an homoclinic saddle connection is trespassed corresponding to phase space transition on two-torus from stable cross-well QP1M2$^{(S)}$ motion to two stable in-well QP1M2$^{(SC)}$ motions.

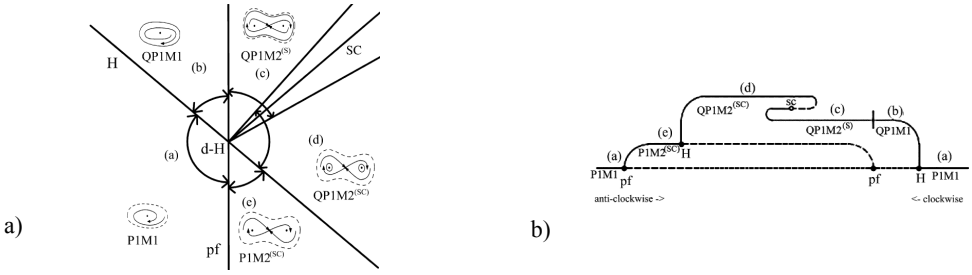

Figure 5: Schematic (a) stability diagram, (b) experimental bifurcation paths.

In turn, *transition to nonregular dynamics* is summarized as follows. Two homoclinic bifurcations responsible for onset of nonregular dynamics from either symmetric (QP1M2$^{(S)}$) or symmetric couple (QP1M2$^{(SC)}$) quasiperiodic response may occur.

Homoclinic explosions originate a strange invariant set that becomes an attractor in a range of control parameters (within the instability range of P1M1), and then suddenly disappears. It is conjectured (see the schematic stability diagram and bifurcation paths in Fig. 6) that, far away from d-H point in the stability diagram (Fig. 6a), the saddle connection locus reaches a *new codimension 2 bifurcation point* (G) where it splits into an *homoclinic explosion/implosion pair*, with an interval of stable nonregular dynamics in between. To make the experimental bifurcation scenario consistent with an interpretative theoretical scheme [4], other bifurcation branches are requested to emanate from G.

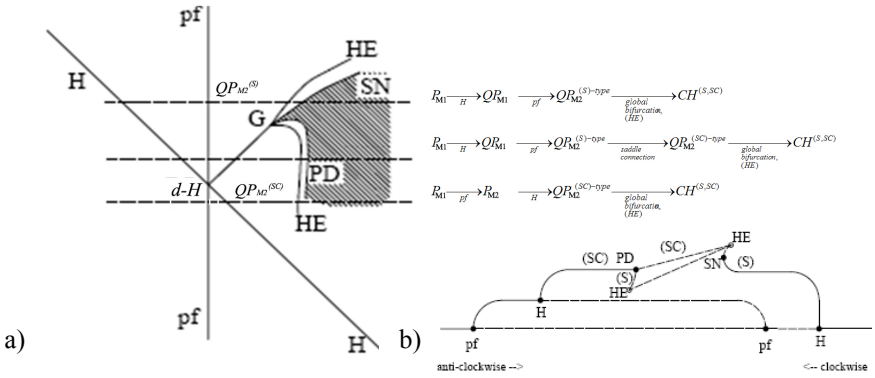

Figure 6: Schematic (a) stability diagram, (b) experimental bifurcation paths.

In such a case (compare with also the bifurcation paths in Fig. 6b): Moving anticlockwise around G: (i) a PD bifurcation on (SC)-cycle (which becomes unstable) produces an unstable (S)-cycle branch reaching an homoclinic explosion (HE) where a strange invariant set is produced, another HE (herein playing an implosion role) then destroying all unstable orbits; (ii) the new born unstable (S)-cycle gains stability due to a SN bifurcation and emerges on the other side of the chaotic region. In turn, moving clockwise around G: (i) a SN bifurcation on (S)-cycle (which becomes unstable) produces an unstable (SC)-cycle branch reaching an homoclinic explosion (HE) where a strange invariant set is produced, another HE then destroying all unstable orbits; (ii) the new born unstable (SC)-cycle gains stability due to PD bifurcation and emerges on the other side of the chaotic region.

3 THE LOW-DIMENSIONAL PHENOMENOLOGICAL MODEL

We aim at building a complete phenomenological model embedding the experimental bifurcation scenario and suitable: (i) to analyze the interaction between the system parameters (linear frequency σ and dissipation μ) governing the unfolding of the normal form of the conjectured codimension 2 bifurcation and the applied excitation amplitude; (ii) to highlight the symmetry breaking effect induced in the unforced system by the asymmetric boundary conditions (sole in-plane support motion) of the experimental system.

The experimental scenario is reproduced using a bifurcation set obtained through the forced symmetry breaking of a highly degenerated normal form of the O(2) symmetric nilpotent double-zero bifurcation. Besides *globally* tracing the experimental scenario, the model has a discrete mathematical structure to be profitably compared with literature cable models. In detail, we need (i) to consider an equation set order corresponding to the experimental response dimensionality; (ii) to respect the symmetry properties of the forced experimental system, which is solely Z2 symmetric instead of being O(2) symmetric as the unforced system in the background. The model is built by reproducing the bifurcation scenario as highlighted in the experimental Poincaré section; yet, the equation set governing the dynamics of the flow is obtained, too.

3.1 *Highly degenerated bifurcation set*

An approach is followed which allows us to build a model possessing not only a higher dimensionality with respect to that of the sole divergence-Hopf bifurcation (marginal stability space of dimension 3) but also a more convenient structure where terms and coefficients preserve a direct physical meaning. First, an O(2) symmetric highly degenerated nilpotent double zero bifurcation set (marginal stability space of dimension 4) is produced. Indeed, if the cable sag-to-span ratio is small, as assumed herein, the unforced physical system has O(2) symmetry properties, and the same features are required to the unforced model in the invariant space spanned by the first two antisymmetric modes (of amplitudes u_1, u_2) where the experimental dynamics we want to reproduce is confined. Then, this symmetry is broken down to Z2 as in the forced physical system, by imposing forcing non- O(2) symmetric boundary conditions to the assumed underlying flow.

The unfolding of the nilpotent double-zero normal form occurring at $\sigma = 0, \mu = 0$, reads, in the O(2) symmetric case and for long times, small amplitudes and small dampings [6]

$$
\begin{aligned}
&\dot{u}_h = v_h \\
&\dot{v}_h = \sigma_h u_h + \mu_h v_h + a_h u_h (u_h{}^2 + u_k{}^2) + c_h v_h \left(u_h{}^2 + u_k{}^2\right) + d_h u_h \left(u_h v_h + u_k v_k\right) \\
&\left(\sigma_h, \mu_h\right) = \left(\sigma_k, \mu_k\right),\ \left(a_h, c_h, d_h\right) = \left(a_k, c_k, d_k\right) \\
&\left(h,k\right) = \left(1,2\right),\left(2,1\right)
\end{aligned}
\tag{1}
$$

To produce the highly degenerated bifurcation set, a third control parameter (the temperature) is introduced – besides the forcing amplitude and frequency – through the following assumptions on the dissipation terms, $\mu = \bar{\mu}\gamma_\mu(T-T_0)+\hat{\mu}$, $c = \bar{c}\gamma_c(T-T_0)$, $d = \bar{d}\gamma_d(T-T_0)$, $e = \bar{e}\gamma_e(T-T_0)$, where $\hat{\mu}$ is the viscous damping, $\bar{\mu},\bar{c},\bar{d},\bar{e}$ are hysteretic coefficients, T is the system ambient temperature and T_0 is its reference value nominally corresponding to the solely viscous dissipation; the temperature dependent γ functions are assumed to vanish, i.e., $\gamma_\mu = \gamma_c = \gamma_d = \gamma_e = 0$, when $T = T_0$. The highly degenerated bifurcation set reads:

$$
\begin{aligned}
&\dot{u}_h = v_h \\
&\dot{v}_h = \sigma_h u_h + (\bar{\mu}_h\gamma_\mu + \hat{\mu}_h)v_h + a_h u_h(u_h^2 + u_k^2) + (\bar{c}_h\gamma_c)v_h\left(u_h^2 + u_k^2\right) + (\bar{d}_h\gamma_d)u_h\left(u_h v_h + u_k v_k\right) + \\
&\qquad (\bar{e}_h\gamma_e)v_h\left(u_h^4 + u_k^4\right)
\end{aligned}
\tag{2}
$$

$$
\left(\sigma_h,\bar{\mu}_h,\hat{\mu}_h\right) = \left(\sigma_k,\bar{\mu}_k,\hat{\mu}_k\right),\left(a_h,c_h,d_h,e_h\right) = \left(a_k,c_k,d_k,e_k\right) \qquad (h,k) = (1,2),(2,1) \tag{2.1}
$$

Note that, on passing from eq. (1) to eq. (2), the homogeneous bifurcation set has been enriched with fifth order terms. Indeed, a partial unfolding of the Z2 symmetric version of eq. (2) obtained by considering different *h* and *k* coefficients, preliminarily performed to verify the possibility to reproduce the experimental scenario and to find the relevant condition on the unfolding parameters, has shown the necessity to break the symmetry of third order terms: the fifth order terms will indeed produce cubic parametric terms breaking the symmetry when non-homogeneous boundary condition will be applied.

3.2 *Periodically excited highly degenerated bifurcation set*

The constructed highly degenerated bifurcation set, eq. (2), can be regarded as the reduced equations (map) of an autonomous evolution equation (flow) of the type $dU/dt = F(\lambda,U)$, where $U \in$ phase space $E = \Re^n$, λ is a vector of control parameters in $\Re^m$, $F(0,0) = 0$ and $L = DF(0,0)$ is the jacobian matrix with a spectrum consisting of eigenvalues with either zero or negative real part. Aiming at reproducing the effect of the support motion in the experimental setup, we look for a reduced bifurcation set of a perturbed evolution equation $dU/dt = F(\lambda,U) + \delta G(\lambda,U,t)$, where δ is the excitation amplitude and $G(\lambda,U,t)$ is a time-periodic perturbation such to break the O(2) symmetry. Note that we know the reduced bifurcation set (2) but we don't know the autonomous evolution set, to be perturbed, in the background.

In order to produce the reduced bifurcation set, considering a generic autonomous evolution set at bifurcation, the phase space *E* is split into its critical and non critical eigenspaces $E_o \oplus E_-$, with corresponding invariant subspaces L_o and L_-. If the *E* phase space dimension of the autonomous evolution set is equal to the critical eigenspace at bifurcation $(E = E_o)$ and the dynamic matrix is already in Jordan canonical form $(L = L_o)$, the perturbed bifurcation set can be obtained, without loss of generality, by assuming the underlying evolution equation just in the form of its (autonomous) reduced bifurcation set, i.e. in the form (2), properly perturbed.

To this aim, the set (2) is enriched (i) by accounting for the effect of a non homogeneous boundary condition, via a suitable coordinate transformation, and (ii) by imposing fulfilment of D4 symmetry properties to the perturbed set of discrete evolution equations. The following perturbed evolution equation set, truncated at third order, is obtained:

$$
\begin{aligned}
&\dot{u}_h = v_h \\
&\dot{v}_h = \sigma u_h + (\bar{\mu}\gamma_\mu + \hat{\mu})v_h + a u_h(u_h^2 + u_k^2) + a\left[3u_h u_{h0}^2 + u_h u_{k0}^2\right] + (\bar{c}\gamma_c)v_h\left(u_h^2 + u_k^2\right) + \\
&(\bar{c}\gamma_c)\left[v_h\left(u_{h0}^2 + u_{k0}^2\right) + 2u_h u_{h0}\dot{u}_{h0}\right] + (\bar{d}\gamma_d)u_h\left(u_h v_h + u_k v_k\right) + (\bar{d}\gamma_d)\left[2u_h u_{h0}\dot{u}_{h0} + u_h u_{k0}\dot{u}_{k0} + u_{h0}^2 v_h\right] + \\
&(\bar{e}\gamma_e)\left[4u_{h0}\dot{u}_{h0}u_h^3 + u_{h0}^2 u_h^2 v_h + 6u_{k0}^2 u_k^2 u_h\right] + \{\ddot{u}_{h0} + (\bar{\mu}\gamma_\mu + \hat{\mu})\dot{u}_{h0}\} + O[u_h]^5 \\
&(h,k) = (1,2),(2,1)
\end{aligned}
\tag{3}
$$

where parametric terms (inside square brackets) as well as inertial and viscous terms (curly brackets) owing to the harmonic support motions $\left(u_{h0} = \delta_h \sin(\Omega t + \varphi),\ h = 1,2\right)$ are recognized.

3.3 *D4 perturbed normal form of the O(2) symmetric nilpotent double-zero bifurcation*

The bifurcation set (3) exhibits for the trivial solution and for $\sigma = \bar{\mu}\gamma_\mu + \hat{\mu} = 0$ a nilpotent double-zero bifurcation. For the sake of deriving a normal form enriched by the contribution of the solely parametric forcing terms and discussing the relevant stability, we apply the multiple time scales method to the equation set (3). The dependent variables u_i are expanded in a fractional series [7] as

$$
u_i(T_0, T_1, T_2, T_3, T_4, T_5) = \sum_{j=0}^{5} \varepsilon^{j/2} u_{i(j)}\left(T_0, T_1, T_2, T_3, T_4, T_5\right) \tag{4}
$$

where $T_j = \varepsilon^j t$, with ε being a smallness parameter.

An ordering of the system terms is done and the perturbation equations at orders $\varepsilon^{j/2}, j = 0,5$ are obtained. They are solved in chain, by imposing the solvability conditions through vanishing of the secular producing terms at orders $\varepsilon^{j/2}, j = 1,5$. The solvability conditions provide the normal form of the equations describing the modulation of the amplitudes and phases of the solution in the slow-varying time scale; in our case, being the system harmonically forced, the aforesaid modulations describe the solution of the parametrically forced flow on the Poincarè section. Primary external and internal 1:1 resonance between in-plane and out-of-plane antisymmetric modes is considered and the normal form reads

$$
\begin{aligned}
&\dot{u}_h = v_h \\
&\dot{v}_h = \left(\sigma + \sigma_h^{(f)}\right)u_h + \left(\bar{\mu}\gamma_\mu + \hat{\mu} + \mu_h^{(f)}\right)v_h + a u_h\left(u_h^2 + u_k^2\right) + a_h^{(f)}u_h^3 + (\bar{c}\gamma_c)v_h\left(u_h^2 + u_k^2\right) + \\
&\quad (\bar{d}\gamma_d)u_h\left(u_h v_h + u_k v_k\right) + O(u_h)^5 \\
&\sigma_h^{(f)} = \frac{3}{2}a\delta_h^2 + \frac{1}{2}a\delta_k^2 + \left(\frac{\bar{c}\gamma_c\bar{d}\gamma_d}{8} - \frac{9}{32}\frac{a^2}{\Omega^2}\right)\delta_h^4 + \left(\frac{\bar{c}\gamma_c\bar{d}\gamma_d}{16} - \frac{\bar{d}^2\gamma_d^2}{32} - \frac{1}{32}\frac{a^2}{\Omega^2}\right)\delta_k^4 \\
&\mu_h^{(f)} = \left(\frac{3}{4}\left(\bar{c}\gamma_c + \bar{d}\gamma_d\right) - \frac{3}{2}\left(\bar{\mu}\gamma_\mu + \hat{\mu}\right)\right)\delta_h^2 + \left(\frac{3}{4}\bar{c}\gamma_c - \frac{3}{2}\left(\bar{\mu}\gamma_\mu + \hat{\mu}\right)\right)\delta_k^2 \\
&a_h^{(f)} = -\frac{1}{2}a\bar{e}_h\gamma_e\delta_h^2 \\
&(h,k) = (1,2),(2,1)
\end{aligned}
\tag{5}
$$

where the superscript *(f)* denotes parametric coefficients reducing the symmetry of the canonical O(2) nilpotent double-zero normal form to D4.

If the experimental case of solely vertical support motion is considered $(\delta_1 \neq 0, \delta_2 = 0)$, the system (5) becomes Z2 symmetric.

4 PARTIAL UNFOLDING OF THE Z2 NORMAL FORM

The stability of the trivial solution is discussed for the two cases $T=T_o$ and $T>T_o$. (i) In the case $T=T_o$, the linear and nonlinear terms depending on the hysteretic behavior in equation (6) vanish. In the excitation parameter plane (σ, f), if the viscous damping parameter ($\hat{\mu}$) is also set to zero, a nilpotent double zero point (Takens-Bogdanov bifurcation) is found (at $\sigma=f=0$), from which two branches ($f>0$, $f<0$) of divergence locus and two branches of Hopf ($\hat{\mu}=0$, $\sigma<0$, $\sigma>0$) locus do emanate. For $\hat{\mu}\neq 0$, neither TB nor Hopf bifurcation points occur on the trivial solution but only divergence loci are present in the forcing parameter plane (Fig. 7a). (ii) Then, the case of temperature higher than T_o ($T>T_o$) is considered, in which linear and nonlinear terms depending on the hysteretic behavior do occur. In the forcing parameter plane, also the Hopf bifurcation is now possible for the trivial solution and $\mu=\bar{\mu}\gamma_\mu(T-T_0)+\hat{\mu}\neq 0$. Two nilpotent double zero (TB_1 and TB_2 points) are evidenced, too (Fig. 7b). It is worth noting that TB's critical forcing decreases with decreasing linear damping up to laying onto the horizontal axis when $\mu=0$ (TB_1 and TB_2 collide and coincide with the origin when $T=T_0$, $\hat{\mu}=0$).

Keeping the nonlinear hysteretic coefficients ($\bar{c},\bar{d}$) fixed and varying the linear damping (μ), the diagram of Fig. 8 is obtained. The $\alpha(T)$ parameter summarizes qualitatively the effect of temperature variations with $\hat{\mu}=0$ if μ tends to zero faster than ($\bar{c},\bar{d}$) coefficients. On the divergence surface a locus of double zero (TB) points is seen to occur at the intersection with the Hopf surface (not shown in the figure).

Let us follow the bifurcation diagram for a fixed value of $T>T_o$. Fig. 9 shows a behaviour chart with motion classes and bifurcation loci in the external detuning (σ)–support motion amplitude (f) plane. Gray region, delimited by saddle node bifurcations, shows the existence range of the one-mode P1M1 solution, stable in a small region on the left. Takens-Bogdanov (σ, f)=(-0.02, 0.11) and divergence-Hopf (σ, f)=(0.035, 0.05) codimension 2 bifurcation points affect the trivial and periodic (P1M1) solutions, respectively. The divergence and Hopf loci of the trivial solution (labelled pf_1 and H_1, respectively) are reported in the behaviour chart, which also summarizes the stability analysis results of the P1M1 solution by showing the corresponding divergence (pf_2) and Hopf (H_2) loci, and their intersection. With increasing frequency, the divergence involves the second mechanical mode (antisymmetric out-of-plane H2) responsible of the onset of P1M2 motion class in the experiment, whereas the Hopf corresponds to the onset of the experimental quasiperiodic QP1M1 motion class. The intersection of the two loci furnishes the searched codimension 2 divergence-Hopf bifurcation.

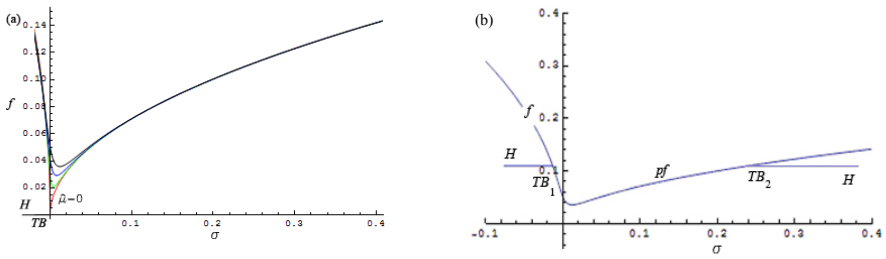

Figure 7: a) $T=T_o$: divergence curves for growing $\hat{\mu}$, TB for $\hat{\mu}=0$; b) $T>T_o$: divergence and Hopf loci intersect at TB bifurcations ($\mu=\bar{\mu}\gamma_\mu(T-T_0)+\hat{\mu}\neq 0$).

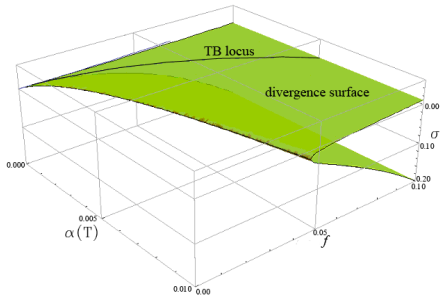

Figure 8: The TB curve in the parameter space $(f, \sigma, \alpha(T))$.

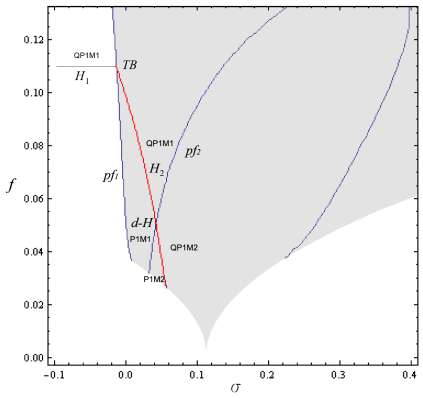

Figure 9: Motion classes and bifurcation loci in the external detuning (σ)–support motion amplitude (f) plane.

5 CONCLUSIONS

Considering the temperature as a further controllable parameter besides the excitation amplitude and frequency has allowed us to interpret the response scenario of an experimental cable-mass system in the neighbourhood of a divergence-Hopf bifurcation in the framework of the symmetry breaking of an highly degenerated bifurcation set describing an O(2) symmetric Takens-Bogdanov bifurcation.

In the context of a profitable feedback between experiments and theory, the phenomenological model has helped steering the experimental analysis and interpreting the relevant results, by also clarifying to which extent they can be referred to a canonical scenario from dynamical systems theory. It also paves the way for improving the continuous cable theoretical modelling and for building reduced order models to be implemented in a numerical procedure for cross-validating and partially reproducing the observed experimental scenarios.

References

[1] Rega G., Nonlinear vibrations of suspended cables. Part I: Modeling and analysis, Part II: Deterministic phenomena. *Appl. Mech. Rev*. 57: 443-514 (2004).

[2] Alaggio R., Rega G., Characterizing bifurcations and classes of motion in the transition to chaos through 3D-tori of a continuous experimental system in solid mechanics. *Physica D* 137: 70-93 (2000).

[3] Rega G., Alaggio R., Spatio-temporal dimensionality in the overall complex dynamics of an experimental cable/mass system. *Int. J. Solids Struct.* 38: 2049-2068 (2001).

[4] Rega G., Alaggio R., Experimental unfolding of the nonlinear dynamics of a cable-mass suspended system around a divergence-Hopf bifurcation. *J. Sound Vibr.* 322: 581–611 (2009).

[5] Troger H., Steindl A., *Nonlinear Stability and Bifurcation Theory*, Springer-Verlag, Wien, 1991.

[6] Armbruster D., Guckenheimer J. and Kim. S., Chaotic dynamics with square symmetry. *Phys. Lett. A* 140: 416-420 (1989).

[7] Luongo A., Paolone A., Di Egidio A., Multiple time scale analysis for bifurcation from a double-zero eigenvalue, *ASME Design Engineering Techn. Conf.*, DETC99/VIB-8053, CD-Rom, 1999.